

## Supplementary Information for

### Recurrent droughts increase risk of cascading tipping events by outpacing adaptive capacities in the Amazon rainforest

N. Wunderling, A. Staal, B. Sakschewski, M. Hirota, O. Tuinenburg, J. Donges, H. Barbosa, R. Winkelmann

Nico Wunderling

E-mail: [nico.wunderling@pik-potsdam.de](mailto:nico.wunderling@pik-potsdam.de)

#### This PDF file includes:

Figs. S1 to S18

SI References

## Methods.

**Computation of the critical function.** While the shape of each cell is represented by Eq. 6, the determination of the critical function with respect to MAP and MCWD remains. The critical function  $\mathcal{F}_{\text{crit}}(\text{MAP}_i, \text{MCWD}_i)$  is computed in two steps. Firstly, for MAP

$$\mathcal{F}_{\text{crit}}(\text{MAP}_i) = \mathcal{C}_{\text{crit}} \cdot \frac{\text{MAP}_i - \mu_{\text{MAP},i}}{\text{MAP}_{\text{crit},i} - \mu_{\text{MAP},i}}, \quad [1]$$

where  $\mu_{\text{MAP},i}$  is the average value of that specific cell over the course of 20 years from the ERA5 calibration dataset (see Supplementary Figs. S8 and S9). The critical value  $\text{MAP}_{\text{crit},i}$  is also computed from this dataset using Eq. 4.  $\text{MAP}_i$  is the actual precipitation value in the cell within the evaluation period, for instance the value of the year 2010 in this cell for the case that the (drought) conditions of the year 2010 are investigated. Secondly, for MCWD

$$\mathcal{F}_{\text{crit}}(\text{MCWD}_i) = \mathcal{C}_{\text{crit}} \cdot \frac{\text{MCWD}_i - \mu_{\text{MCWD},i}}{\text{MCWD}_{\text{crit},i} - \mu_{\text{MCWD},i}}. \quad [2]$$

Although both equations (Eqs. 1 and 2) are in principle not limited, we restrict them to the interval  $[0, \mathcal{C}_{\text{crit}}]$  since the critical value for tipping of Eq. 6 is reached at  $\mathcal{C}_{\text{crit}}$  such that higher values are not necessary to tip a certain cell. Then, the critical function  $\mathcal{F}_{\text{crit}}(\text{MAP}_i, \text{MCWD}_i)$  is computed as

$$\begin{aligned} \mathcal{F}_{\text{crit}}(\text{MAP}_i, \text{MCWD}_i) = & \max\{\mathcal{F}_{\text{crit}}(\text{MAP}_i), \mathcal{F}_{\text{crit}}(\text{MCWD}_i)\} + \\ & + \left(1 - \frac{\max\{\mathcal{F}_{\text{crit}}(\text{MAP}_i), \mathcal{F}_{\text{crit}}(\text{MCWD}_i)\}}{\mathcal{C}_{\text{crit}}}\right) \cdot \\ & \cdot \min\{\mathcal{F}_{\text{crit}}(\text{MAP}_i), \mathcal{F}_{\text{crit}}(\text{MCWD}_i)\}. \end{aligned} \quad [3]$$

Again, the values of Eq. 3 are restricted to the interval  $[0, \mathcal{C}_{\text{crit}}]$  since a state change occurs as soon as the upper value of the interval, i.e.  $\mathcal{C}_{\text{crit}}$ , is reached. To evaluate  $\mathcal{F}_{\text{crit}}(\text{MAP}_i, \text{MCWD}_i)$  in Eq. 3, there are two important cases, which need to be distinguished: (i) *Tipping event occurs*: In a certain grid cell  $i$ , either the value of  $\text{MAP}_i$  or  $\text{MCWD}_i$  (or both) lie beyond their critical value  $\text{MAP}_{\text{crit}}$  or  $\text{MCWD}_{\text{crit}}$ . If this is the case, the respective grid cell  $i$  tips because the first term “ $\max\{\mathcal{F}_{\text{crit}}(\text{MAP}_i), \mathcal{F}_{\text{crit}}(\text{MCWD}_i)\}$ ” in Eq. 3 is larger than  $\mathcal{C}_{\text{crit}}$ . The second term is always positive and does therefore not play a role in this case. (ii) *No tipping event occurs*: In this case  $\mathcal{F}_{\text{crit}}(\text{MAP}_i)$  and  $\mathcal{F}_{\text{crit}}(\text{MCWD}_i)$  are larger or equal to zero, but smaller than  $\mathcal{C}_{\text{crit}}$ . Then, both terms of Eq. 3 are required, where the second term takes the additional effect of the smaller of the two tipping reasons (MAP or MCWD) into account. To better explain this, let us assume that cell  $i$  is drawn closer to its tipping point due to  $\text{MAP}_i$  than it would due to  $\text{MCWD}_i$ , i.e.  $\mathcal{F}_{\text{crit}}(\text{MAP}_i) > \mathcal{F}_{\text{crit}}(\text{MCWD}_i)$ . Then Eq. 3 becomes

$$\begin{aligned} \mathcal{F}_{\text{crit}}(\text{MAP}_i, \text{MCWD}_i) = \\ \mathcal{F}_{\text{crit}}(\text{MAP}_i) + \left(1 - \frac{\mathcal{F}_{\text{crit}}(\text{MAP}_i)}{\mathcal{C}_{\text{crit}}}\right) \cdot \mathcal{F}_{\text{crit}}(\text{MCWD}_i). \end{aligned} \quad [4]$$

Therefore, Eq. 3 allows to distinguish every two different cells  $i$  and  $j$  in their critical values, in case they do not have the exact same MAP and MCWD values. This is an advantage of our fully dynamic model, whereas threshold-only models would not be capable of doing this.

As a concrete example, let us imagine two Amazon rainforest grid cells  $i$  and  $j$ , where  $\text{MAP}_i = 1000$  mm/yr and  $\text{MCWD}_i = 100$  mm/yr, and  $\text{MAP}_j = 1000$  mm/yr and  $\text{MCWD}_j = 200$  mm/yr. For both grid cells, the leading critical value is assumed to be MAP and Eq. 4 is valid. In this case it is sensible that Eq. 3 does not lead to the same value, but the grid cell  $j$  is closer to the critical value than grid cell  $i$  because the MCWD value of  $j$  is larger than that of  $i$ . Eq. 3 is therefore tailored to assign a unique value  $\mathcal{F}_{\text{crit}}(\text{MAP}_{i/j}, \text{MCWD}_{i/j})$  to each unique pair of  $\text{MAP}_{i/j}$  and  $\text{MCWD}_{i/j}$ .

**Computation of the critical matrix.** In analogy to Eqs. 1 and 2, we define the critical matrix for MAP as

$$\mathcal{M}_{ji}(\Delta\text{MAP}_{ji}) = \frac{\mathcal{C}_{\text{crit}} \cdot \Delta\text{MAP}_{ji}}{\text{MAP}_{\text{crit},i} - \mu_{\text{MAP},i}} := \mathcal{M}_{ji, \text{MAP}}, \quad [5]$$

where  $\Delta\text{MAP}_{ji}$  represents the difference of the mean annual precipitation arising from the atmospheric moisture recycling link  $\delta_{ji}$  from cell  $j$  to cell  $i$ . Thus:  $\Delta\text{MAP}_{ji} = \Delta\text{MAP}(\delta_{ji}) = \delta_{ji, \text{MAP}}$ .

For MCWD we have

$$\mathcal{M}_{ji}(\Delta\text{MCWD}_{ji}) = \frac{\mathcal{C}_{\text{crit}} \cdot \Delta\text{MCWD}_{ji}}{\text{MCWD}_{\text{crit},i} - \mu_{\text{MCWD},i}} := \mathcal{M}_{ji, \text{MCWD}}, \quad [6]$$

where  $\Delta\text{MCWD}_{ji} = \Delta\text{MCWD}(\delta_{ji, \text{MAP}})$  is the potential increase of MCWD in response to the atmospheric moisture recycling link  $\delta_{ji, \text{MAP}}$  from cell  $j$  to cell  $i$ . Note that the atmospheric moisture recycling link  $\delta_{ji, \text{MAP}}$  can reduce the precipitation, while the evapotranspiration (which also goes into the computation of the MCWD value, see Eq. 1) remains constant. Also further changes such as in the latent heat flux might affect precipitation changes, but this is beyond the scope of this research to be fully quantified here. However, the effect of atmospheric heat transfer is fundamentally different in the sense that radiation

effects dominate the heat transport, while that is not the case for moisture transport. Due to this difference, the heat transport effects are probably more relevant during shorter, extreme events when the radiative processes are relatively small compared to the length of the event. Because moisture recycling is not affected by radiative effects, moisture recycling effects are important during both extremes and climatological mean periods. Therefore, we have concentrated on quantifying these processes, as this work focuses on the climatological mean effects.

Analogously to Eq. 3, the complete critical matrix is computed as

$$\begin{aligned} \mathcal{M}_{ji}(\Delta\text{MAP}_{ji}, \Delta\text{MCWD}_{ji}) &= \\ &= \mathcal{M}_{ji, \text{MAP}} + \left(1 - \frac{\mathcal{M}_{ji, \text{MAP}}}{\mathcal{C}_{\text{crit}}}\right) \cdot \mathcal{M}_{ji, \text{MCWD}} \end{aligned} \quad [7]$$

if  $\mathcal{F}_{\text{crit}}(\text{MAP}_i) > \mathcal{F}_{\text{crit}}(\text{MCWD}_i)$  or

$$\begin{aligned} \mathcal{M}_{ji}(\Delta\text{MAP}_{ji}, \Delta\text{MCWD}_{ji}) &= \\ &= \mathcal{M}_{ji, \text{MCWD}} + \left(1 - \frac{\mathcal{M}_{ji, \text{MCWD}}}{\mathcal{C}_{\text{crit}}}\right) \cdot \mathcal{M}_{ji, \text{MAP}} \end{aligned} \quad [8]$$

if  $\mathcal{F}_{\text{crit}}(\text{MAP}_i) < \mathcal{F}_{\text{crit}}(\text{MCWD}_i)$ .

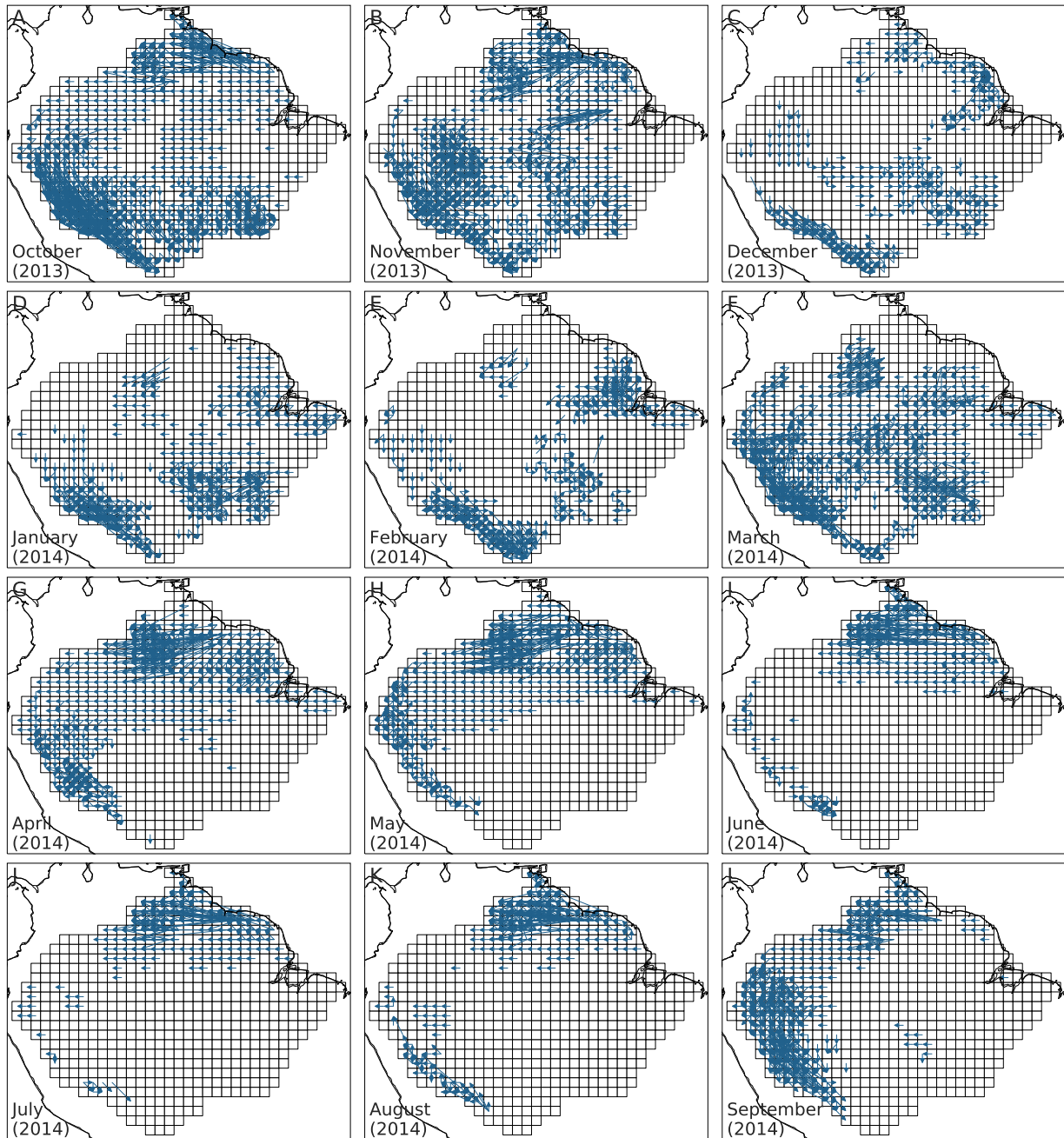


**Fig. S1.** Atmospheric moisture recycling network 2014. (A–L) Monthly atmospheric moisture recycling network links with a strength of 2 mm/month or above. This threshold has been chosen to preserve visibility. Values are shown for the hydrological year 2014, i.e., from October 2013 (panel (A)) to September 2014 (panel (L)). Compare to drought year 2010 (see Supplementary Fig. S2) and dry/wet season flows (see Supplementary Fig. S3).

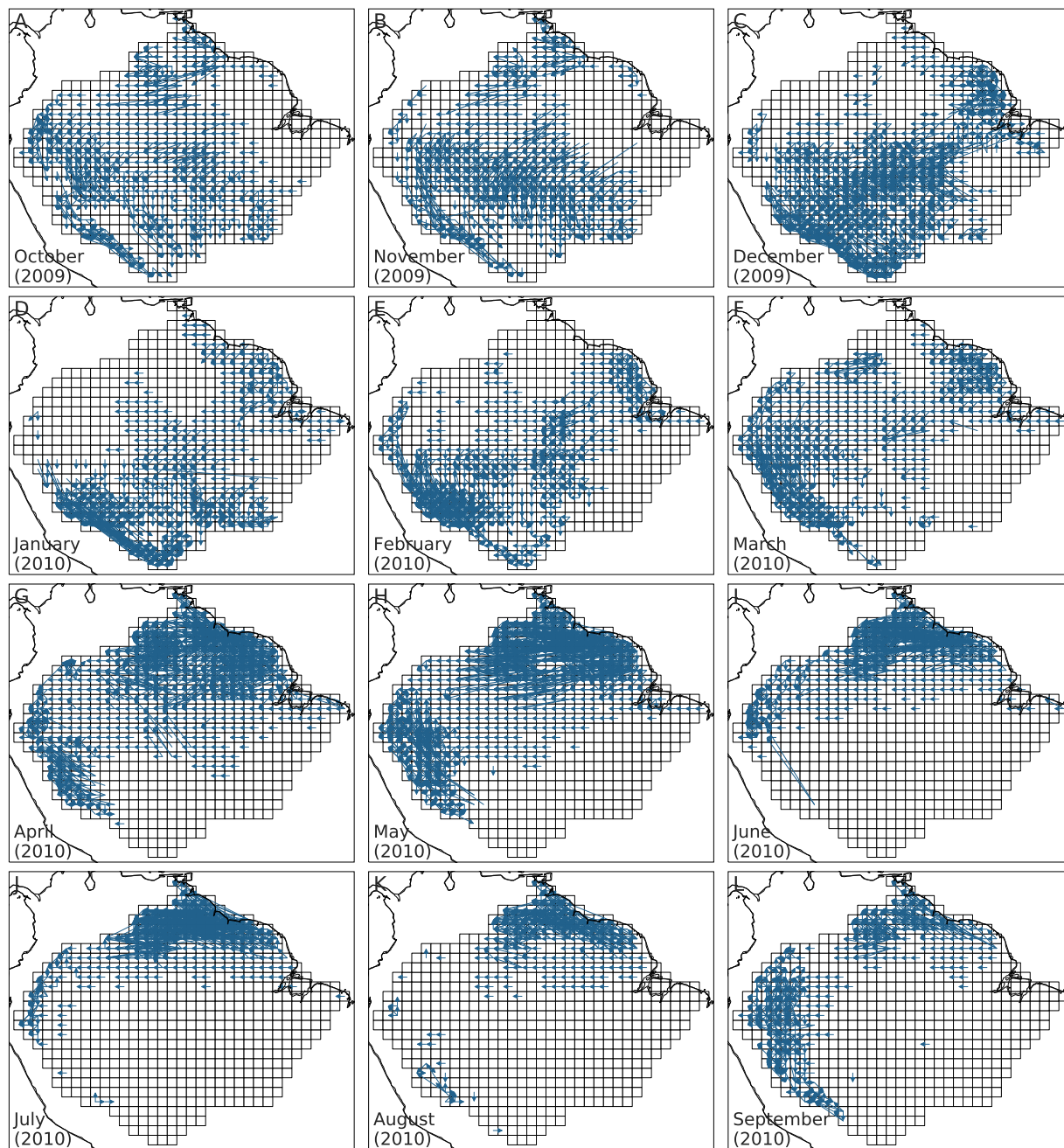


**Fig. S2.** Atmospheric moisture recycling network 2010. (A–L) Monthly atmospheric moisture recycling network links with a strength of 2 mm/month or above. Values are shown for the drought year 2010. Panel (A) represents October 2009 and panel (L) represents September 2010. Compare with Supplementary Fig. S1 for the year 2014 and with dry/wet season flows in Supplementary Fig. S3.

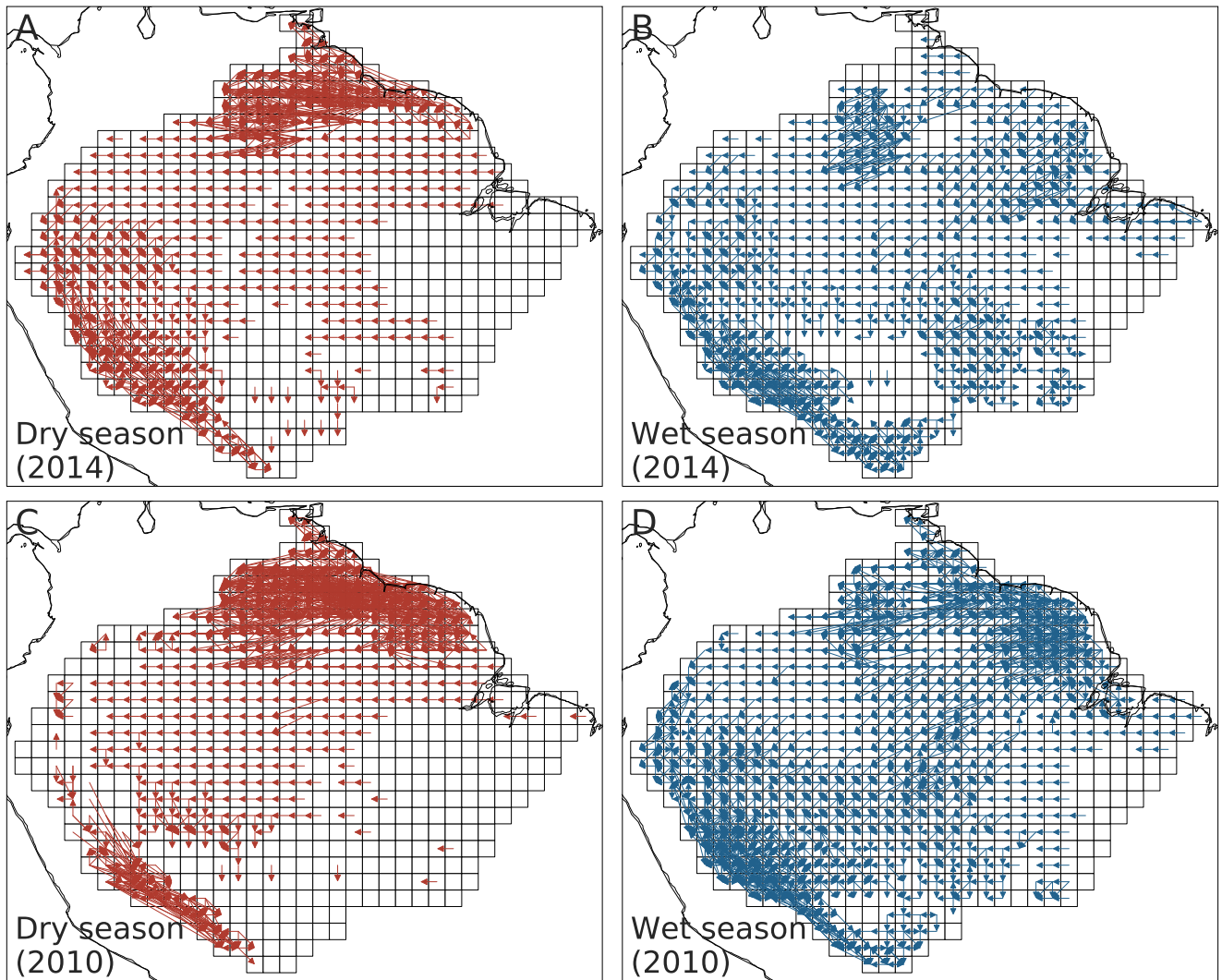


**Fig. S3.** Atmospheric moisture recycling network for the dry and the wet season. Monthly atmospheric moisture recycling network links with a strength of 7.5 mm/month or above. This threshold has been chosen to preserve visibility. Values are shown for (A) dry season (June–November) in 2014, (B) wet season (December–May) in 2014, (C) dry season in 2010, (D) wet season in 2010. Dry and wet season months have been defined according to Zemp et al. (2017) (1), but note those authors considered a year-averaged atmospheric moisture recycling network.

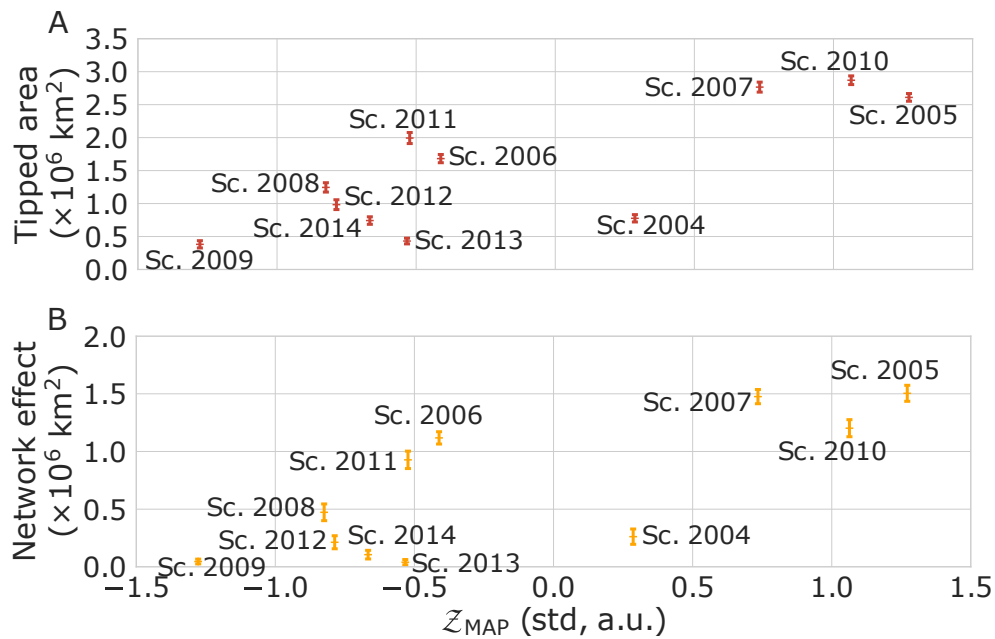


**Fig. S4.** Vulnerability of the rainforest against a MAP-based  $Z$ -score. (A) The total tipped area is shown over the course of the mean annual precipitation based  $Z$ -score measured in standard deviations in analogue to the MCWD drought index (see main manuscript's Fig. 2). (B) The additional tipped area due to network effects for each scenario year (future climate normal). Over the course of the study period, we probe a range from around  $-1.5$  to  $+1.5$  standard deviations of precipitation, i.e., on average, wetter years than in the calibration/experience period from 1984–2003. The error depicts the standard deviation over the entire ensemble for each scenario year (cf. methods: *Ensemble construction*; Sc.=Scenario).

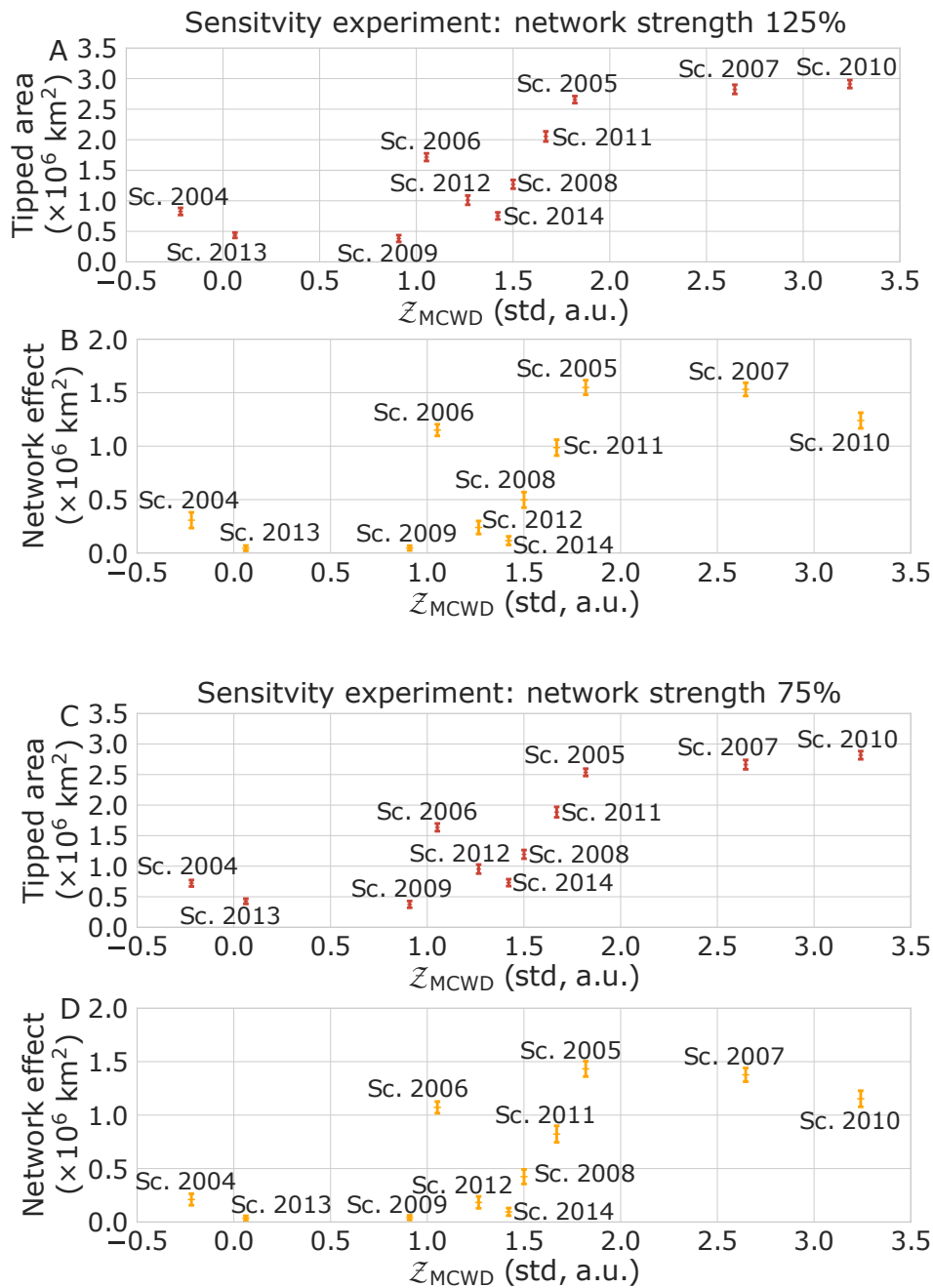


**Fig. S5.** Sensitivity experiment with respect to the tipped area and the strength of the network effect. (A, B) Same as in Fig. 2 of the main manuscript, but with a stronger atmospheric moisture recycling network (each link multiplied by 125%, i.e. remaining ET after tree removal is 25% smaller). (C, D) Same as in Fig. 2, but with a weaker atmospheric moisture recycling network (each link multiplied by 75%, i.e. remaining ET after tree removal is 25% larger). The results remain robust within their standard deviations (error bars). The corresponding remaining evapotranspiration (ET) values can be found in Supplementary Fig. S10 in panels (C) (125% network strength, i.e. remaining ET after tree removal is 25% smaller) and (D) (75% network strength, i.e. remaining ET after tree removal is 25% larger).

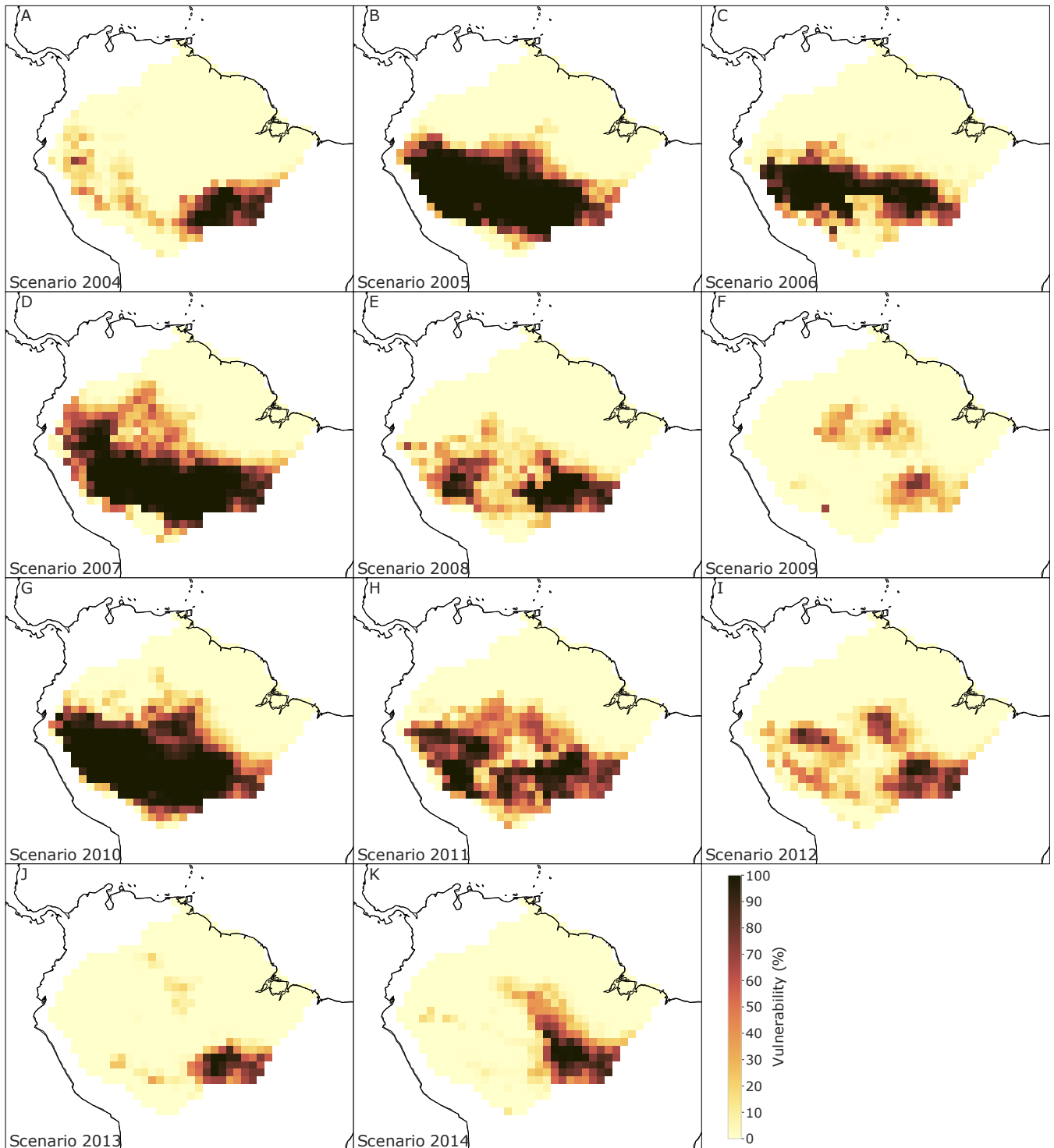


**Fig. S6.** Endangered regions for each simulated scenario. Risk maps for the likelihood of instabilities for the different simulated scenarios, corresponding to hydrological years 2004 (panel (A)) to 2014 (panel (K)). The mean of these vulnerability maps is shown in the main manuscript (Fig. 3A). For a given grid-point, the vulnerability is the fraction of the times that it was converted from forest to the alternative state (open canopy, savanna, treeless), averaged over all ensemble members. As expected, the drought years 2005, 2007, and 2010 show the highest vulnerability.

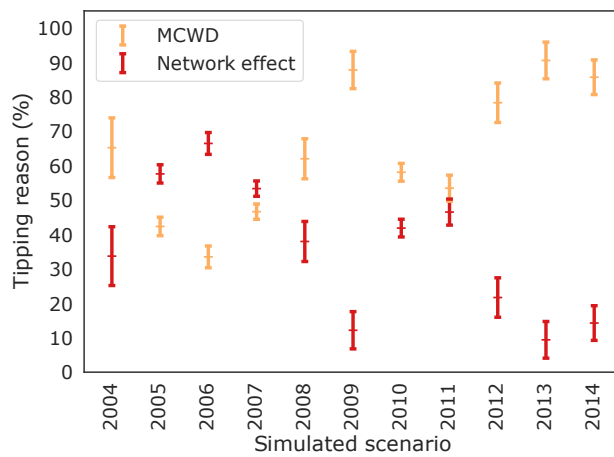


**Fig. S7.** Tipping reason. The importance of two possible tipping reasons (MCWD and network effects: tipping cascades) is shown for the different simulation scenarios corresponding to the hydrological years 2004–2014. Note that tipping cascades (network effects) and direct MCWD induced tipping must add up to 100% since MAP is negligible as a primary tipping reason. Overall, network effects, i.e., cascading effects, account for around 10% to up to 65% of all tipping events. The error bars show the standard deviation over all 100 ensemble members in each year. The mean over all scenarios is shown in the main manuscript in Fig. 3B. MAP as a tipping reason is not shown since MAP as a tipping reason accounts for less than 0.1% overall.

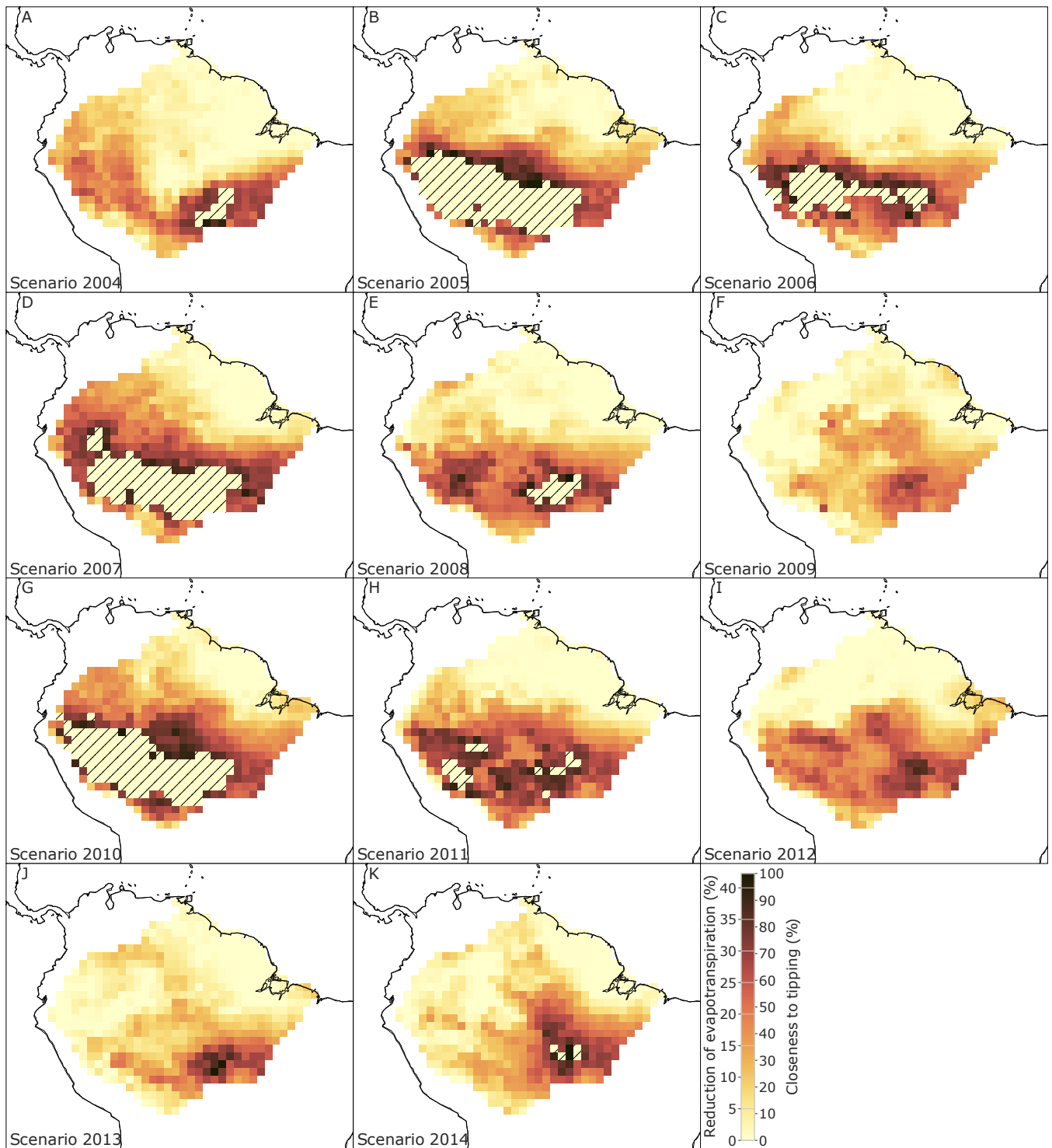


**Fig. S8.** Closeness to tipping for each simulated scenario. Closeness to tipping separated for the different simulated scenarios, corresponding to hydrological years 2004 (panel (A)) to 2014 (panel (K)). The hatched cells in the middle of dark red regions in the southern and southwestern Amazon reflect that these regions are tipped for all 100 ensemble members. At these regions, the closeness to tipping cannot be evaluated since the respective cells are already shifted beyond their tipping point, while the closeness to tipping only measures the average shift towards (but not beyond) the tipping point. The summary of these vulnerability maps is shown in the main manuscript (Fig. 4).

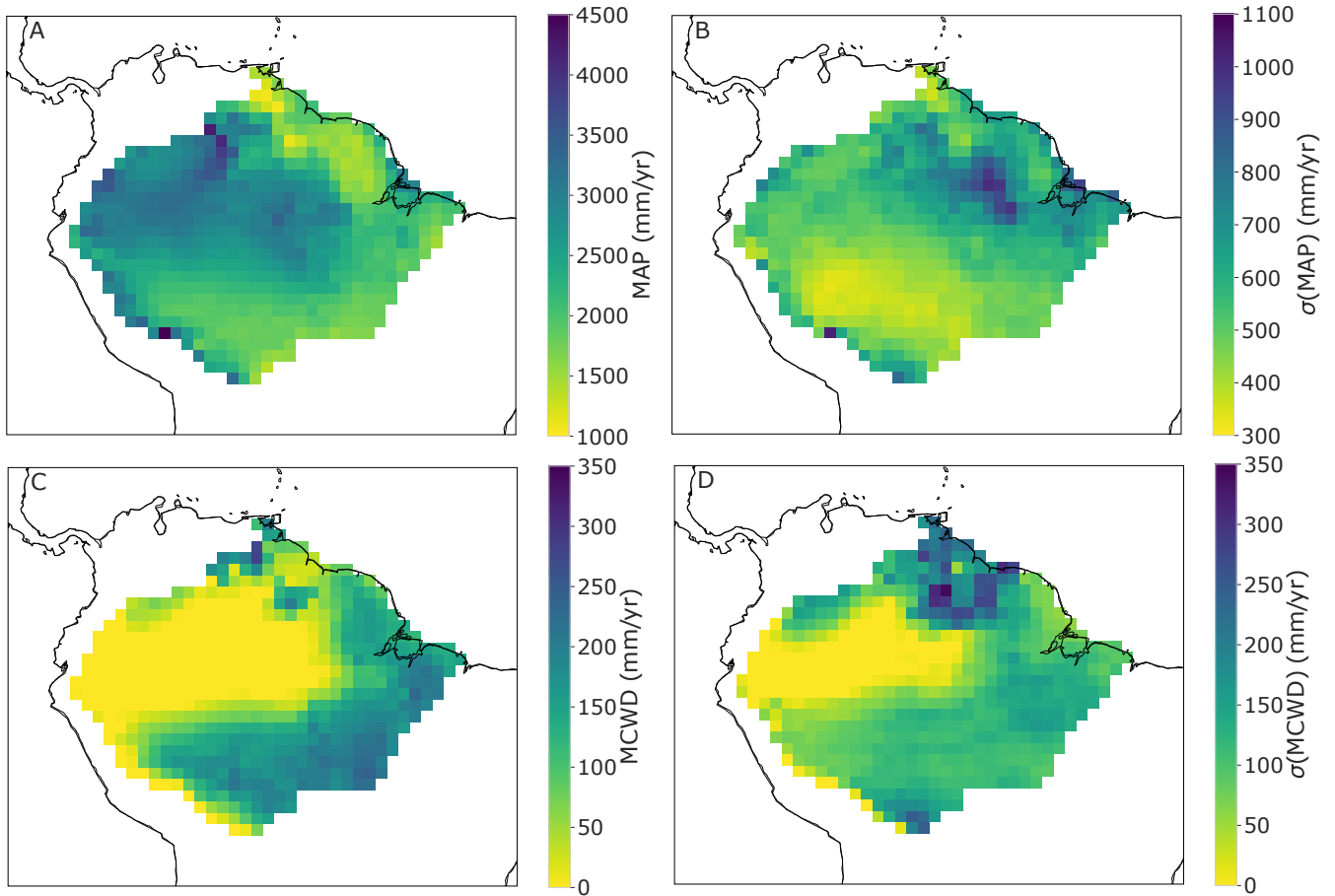


**Fig. S9.** Determination of the critical values. (A) Average mean annual precipitation (MAP), (B) Standard deviation of MAP, (C) Average maximum cumulative water deficit (MCWD), (D) Standard deviation of the average MCWD. All panels show values from the hydrological years 1984–2003 derived from ERA5, which are used to compute the critical values of each grid cell located in the Amazon basin.

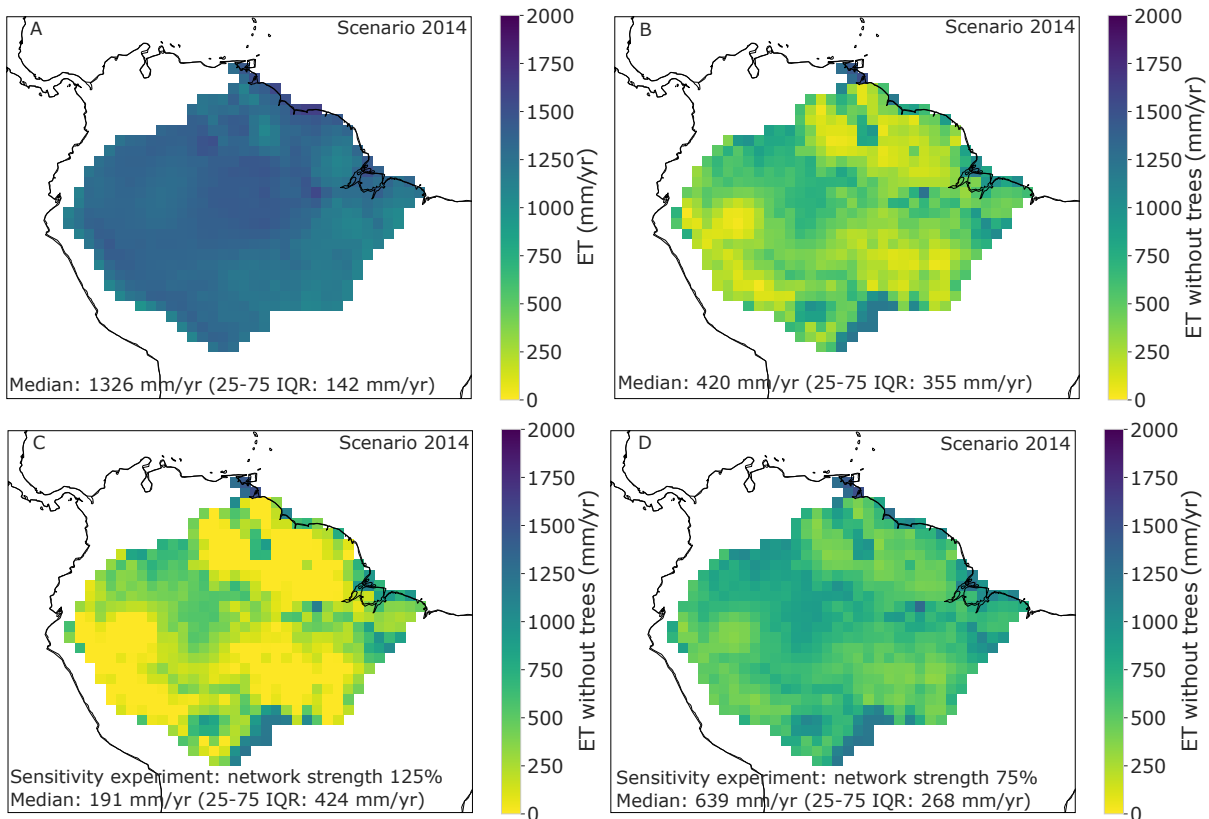


**Fig. S10.** Evapotranspiration with and without tree transpiration and interception evaporation for the hydrological year 2014. (A) Evapotranspiration (ET) with full tree cover including tree transpiration and interception evaporation. (B) ET in case trees in all cells would be removed, without tree transpiration and interception evaporation. (C, D) Remaining ET values in case all atmospheric moisture recycling links (network strength) are multiplied by 125% or 75%, respectively. The remaining ET values match the value of ET for dry forests, or pasture and soy well for the sensitivity experiment in panel (D) (2, 3). Values are shown for the hydrological year 2014, but other years show similar results. The median value of ET is given together with the interquartile range from the 25th to the 75th percentile (25-75 IQR) for each panel. The resulting sensitivity experiments (tipped areas) can be found in Supplementary Fig. S5.

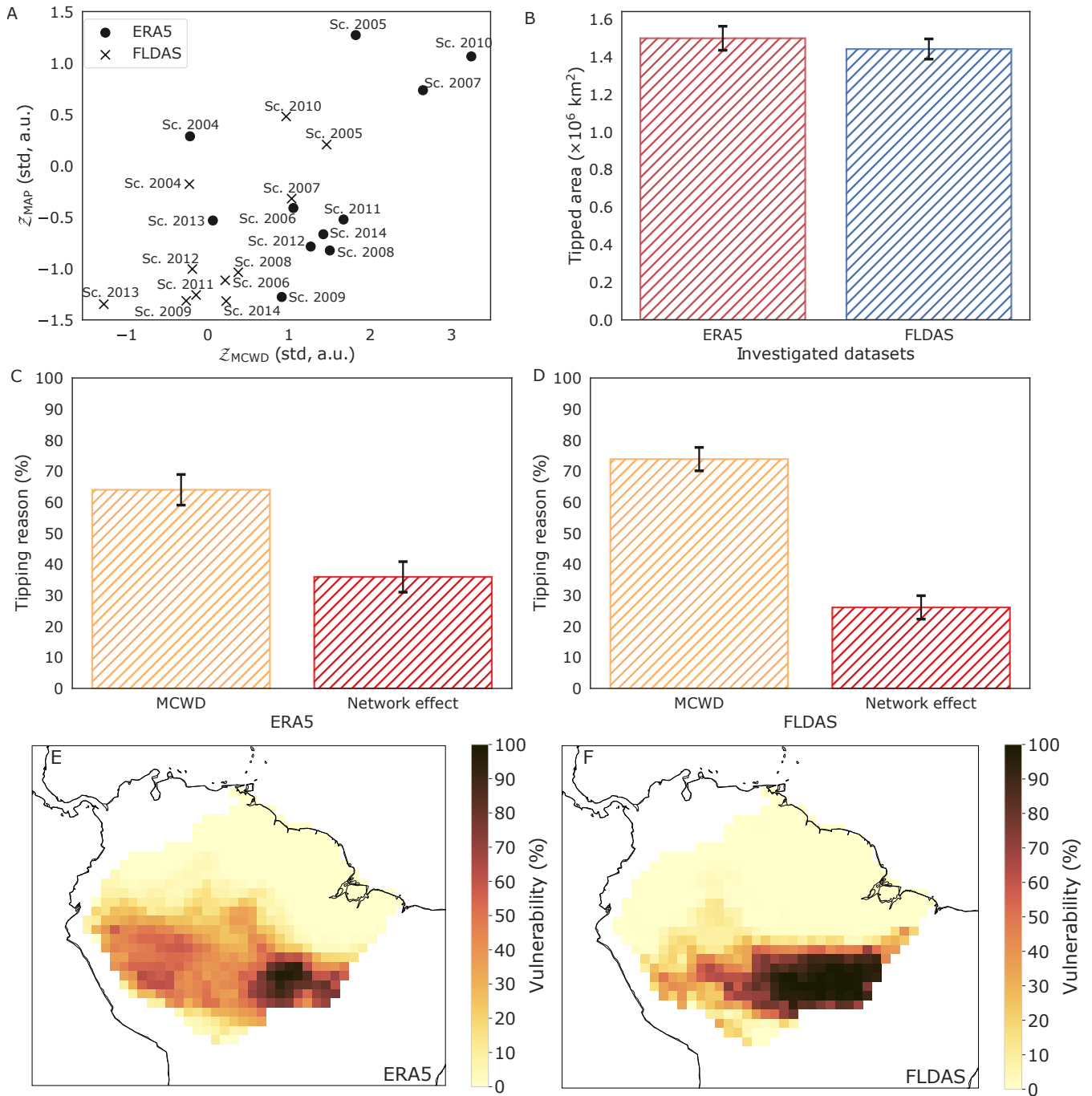


**Fig. S11.** Comparison between ERA5 and FLDAS data (see also supp. Figs. S12 and S13). (A) Plot of all examined scenarios from 2004–2014 as a function of  $Z_{MAP}$  and  $Z_{MCWD}$  (Sc.=Scenario). The spread of environmental conditions in terms of their  $Z$ -score of the ERA5 data (dots) is a bit larger and tends more towards drier years, where  $Z_{MAP}$  and  $Z_{MCWD}$  are higher as compared to the FLDAS data (crosses). (B) The overall tipped area resulting from these different  $Z$ -scores average over all years. Comparing the result for the ERA5 and the FLDAS dataset shows that our results are robust among the two datasets. The tipped area using the ERA5 data is  $1.50 \pm 0.07 \cdot 10^6 \text{ km}^2$ , while it is  $1.44 \pm 0.05 \cdot 10^6 \text{ km}^2$  for the FLDAS data. (C) Tipping reason for the ERA5 data, distributed among MCWD ( $64 \pm 5\%$ ) and MAP ( $36 \pm 5\%$ ). Note that this panel is taken from the main manuscript Fig. 3B to compare to the FLDAS data. (D) Same as for panel (C), but for the FLDAS data. MCWD-induced tipping events are responsible for  $74 \pm 4\%$  of all tipping events, while  $26 \pm 4\%$  are due to network effects (tipping cascades). In both datasets, MAP is no trigger of tipping events, highlighting the consistency of our results. (E) Vulnerable regions for ERA5 data. Note that this panel is taken from the main manuscript Fig. 3A. (F) Vulnerable regions for FLDAS data.

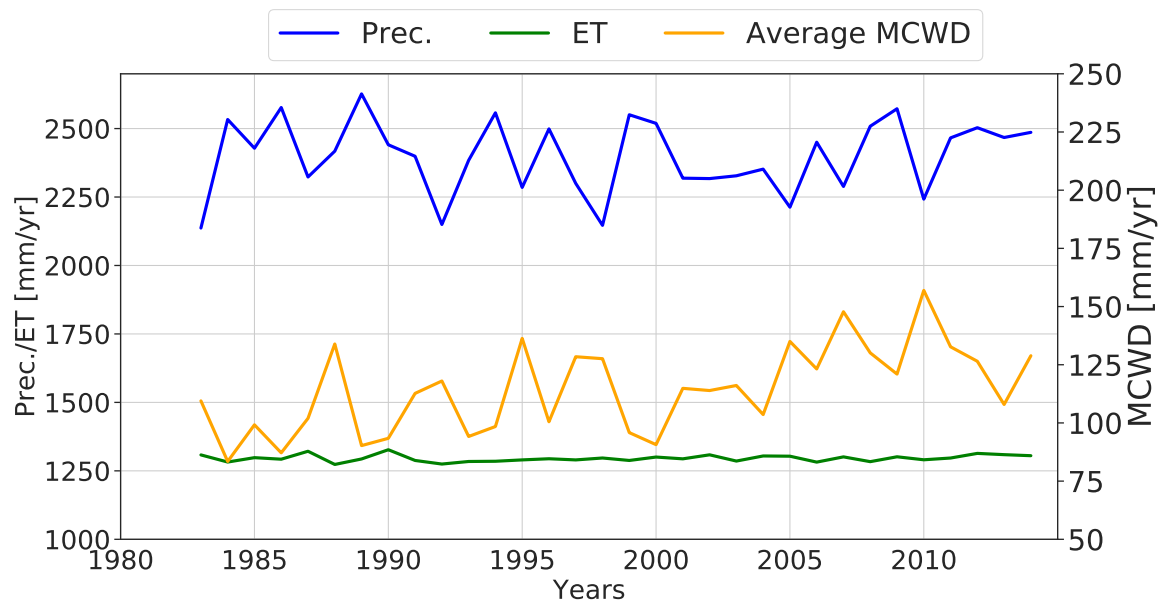


**Fig. S12.** Average precipitation, evapotranspiration and MCWD according to ERA5. Average precipitation (blue) and actual evapotranspiration (ET, green) for the calibration data set (hydrological years 1984–2003) and the evaluation data set (hydrological years 2004–2014). The data is aggregated on a yearly basis and averaged over the whole Amazon basin. The average MCWD is plotted in orange (right y-axis).

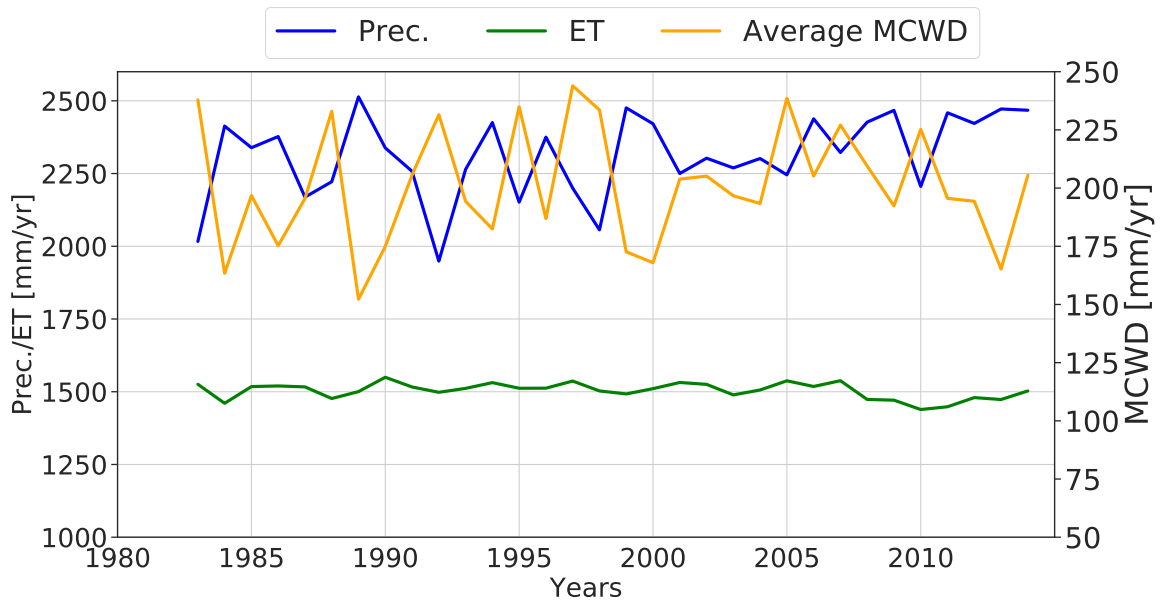
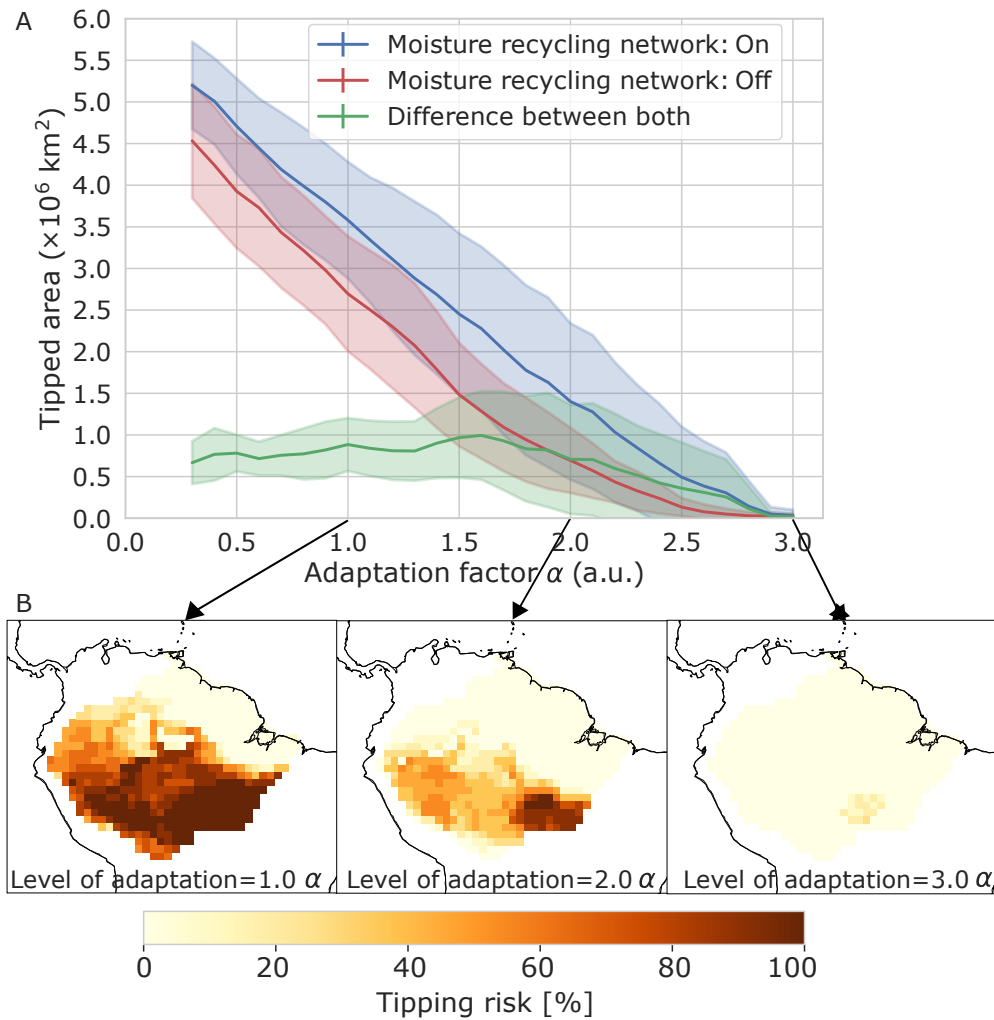
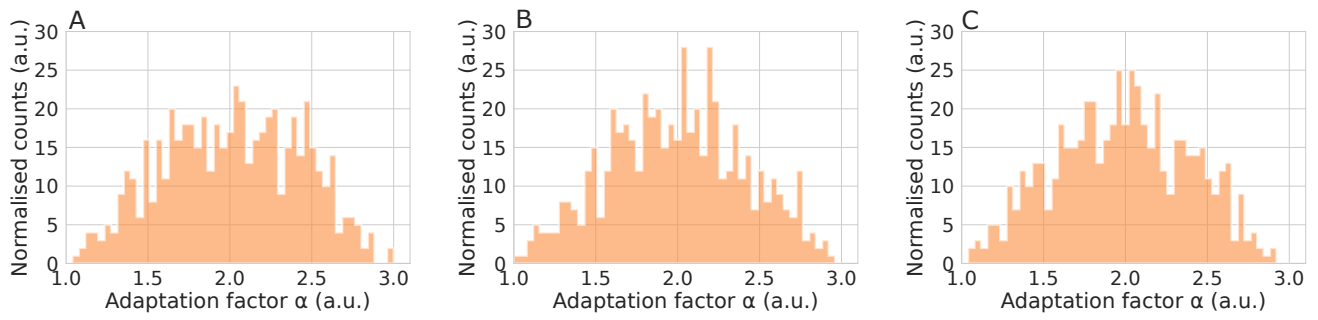


Fig. S13. Same as Fig. S12 before for the FLDAS data instead of the ERA5 data.



**Fig. S14.** Dependence of tipping on the adaptation factor. (A) Tipped area versus adaptation factor, where each cell has the same adaptation factor ( $\alpha_i = \alpha \forall i$ ). The absolute tipped area is shown for an experiment with the atmospheric moisture recycling network (blue) and for comparison without the atmospheric moisture recycling network (red). The absolute difference (green) shows the area that tips due to network effects (tipping cascades). The shaded regions show the standard deviation that arises from the simulations from the hydrological years 2004–2014. (B) Regional distribution of the risk for the occurrence of tipping events if all cells would have an adaptation factor of  $\alpha_i = 3.0 \alpha$  (right panel),  $\alpha_i = 2.0 \alpha$  (central panel), or  $\alpha_i = 1.0 \alpha$  (left panel). It can be seen that the most vulnerable region lies in the south of the Amazon basin (right panel) and spreads to the western Amazon basin with lower adaptation factors (central panel), and afterwards spreading northward at very low adaptation factors (left panel). Following this analysis, the most stable region therefore lies in the northwest of the Amazon basin close to the Atlantic.



**Fig. S15.** Ensemble of starting conditions. (A–C) Three examples of initial conditions for the local adaptation factor  $\alpha_i$  for the 567 cells in the Amazon rainforest basin at a resolution of  $1^\circ \times 1^\circ$ . The values are  $\beta$ -distributed according Eq. 5 in the main manuscript.

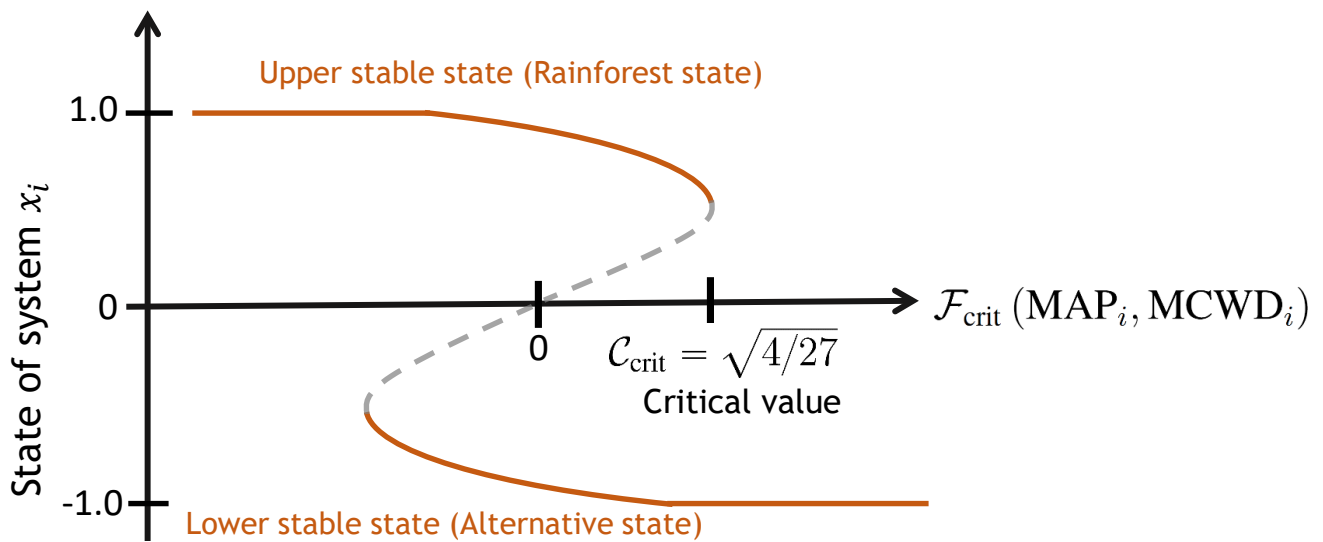


**Fig. S16.** Bifurcation diagram of a grid cell as a tipping element. Stable states of the tipping element  $x_i$  with respect to the critical function  $\mathcal{F}_{\text{crit}}(\text{MAP}_i, \text{MCWD}_i)$ . As soon as the *critical value* is reached, the upper stable branch vanishes and a state transition from the upper to the lower stable state occurs. If the differential equation of the form in Eq. 6 is used, the critical value is analytically representable as  $C_{\text{crit}} = \sqrt{4/27}$ . Due to this reason of analytic representation, an upper state limit of +1.0 (representing the rainforest state) and a lower state limit of -1.0 (the alternative state) is chosen.

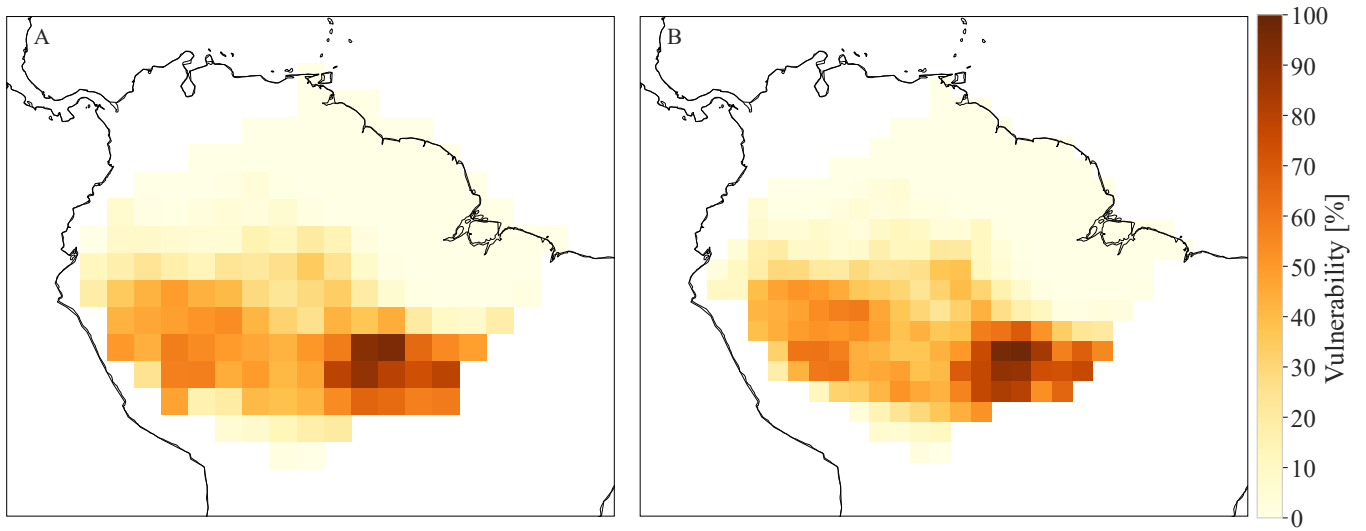


**Fig. S17.** Resolution dependence. Same as Fig. 3A in the main manuscript, but for a resolution of (A)  $2^\circ \times 2^\circ$  and (B) for a resolution of  $1.5^\circ \times 1.5^\circ$ . We find quantitative agreement with the results in Fig. 3A (see also Supplementary Fig. S18). For a given grid-point, the vulnerability is the fraction of the time that it was converted from forest to savanna, averaged over all ensemble members.

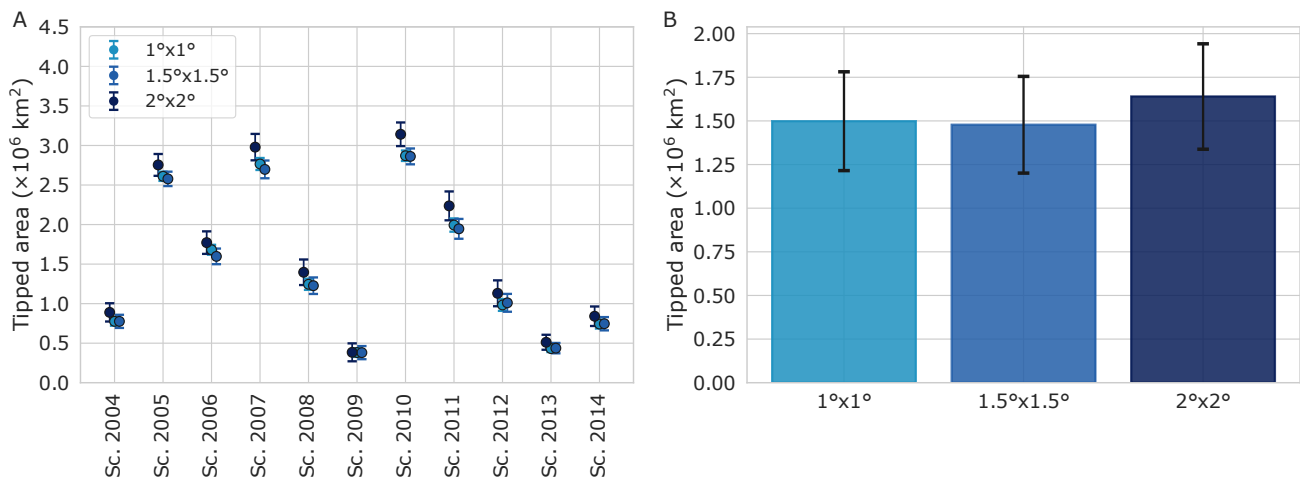


**Fig. S18.** Absolute resolution dependences. (A) Tipped area for all investigated resolutions ( $1^\circ \times 1^\circ$ ,  $1.5^\circ \times 1.5^\circ$ ,  $2^\circ \times 2^\circ$ ). Error bars show the standard deviation over the 100 ensemble members for each scenario (representing the hydrological years 2004–2014). (B) Summary of panel (A) over all scenarios. Error bars show the standard deviation over all scenarios in panel (A). We find quantitative agreement between the different resolutions within their error bars.

## References

1. DC Zemp, et al., Self-amplified Amazon forest loss due to vegetation-atmosphere feedbacks. *Nat. Commun.* **8**, 14681 (2017).
2. M Jung, et al., Recent decline in the global land evapotranspiration trend due to limited moisture supply. *Nature* **467**, 951–954 (2010).
3. G de Oliveira, et al., Evapotranspiration and precipitation over pasture and soybean areas in the Xingu River basin, an expanding Amazonian agricultural frontier. *Agronomy* **10**, 1112 (2020).